Microbeam synchrotron imaging of hairs from Ancient Egyptian mummies

L. Bertrand,[a]*† J. Doucet,[b] P. Dumas,[b] A. Simionovici,[c] G. Tsoucaris[a] and P. Walter[a]

[a]Centre de Recherche et de Restauration des Musées de France, UMR 171 du CNRS, 6 Rue des Pyramides, Paris, France, [b]Laboratoire d'Utilisation du Rayonnement Électromagnétique, Bâtiment 209D, Université Paris-Sud, Orsay, France, and [c]European Synchrotron Research Facility, Beamline ID22, 6 Rue Jules Horowitz, BP 220, Grenoble, France. E-mail: loic.bertrand@m4x.org

Developments in microfocus synchrotron techniques have led to new results regarding the long-term alteration of archaeological samples of biological origin. Here, ancient hair samples from two Egyptian mummies have been analyzed using a conjunction of structural and elemental synchrotron methods. In this favored context of conservation, structural analysis revealed a remarkable preservation of keratin supramolecular organization at any observed length scale. Bulk keratin structure has therefore not been modified significantly over 2000 years. However, infrared spectroscopy indicated a partial disorganization of keratins close to the hair surface through polypeptide bond breakage. Elemental mapping showed a strongly heterogeneous distribution which can be related to mummification and cosmetic treatments.

Keywords: synchrotron imaging; microbeam; hair; archaeology; keratin.

1. Introduction

Human hair is a keratinized fiber with a diameter of 50–100 µm. Its cross section can be divided into three main concentric structural zones from the center to the periphery: medulla, cortex and cuticle. Hair cortex represents an average of 90% of the total hair mass. It consists of tightly packed 100 µm-long cells (keratinocytes) that are separated by an intercellular lipido-proteinic matrix. Keratinocytes are mostly filled with keratin intermediate filaments embedded in an inter-filamentous protein material. Keratins are characterized by a succession of organized supramolecular assemblies of increasing size, on scales ranging from one nanometer to several micrometers. Intermediate filaments are themselves arranged according to a quasi-regular hexagonal pattern, described as paracrystalline (Hosemann & Bagchi, 1962). It is this intricate strongly oriented supramolecular organization that confers to hair and epidermis their important function of protective barrier against chemical, mechanical and physical aggressions (Garson *et al.*, 1991; Briki *et al.*, 1998). Keratin and organized lipid structures can both be studied by small-angle X-ray diffraction techniques (Fraser *et al.*, 1963, 1986).

Hair and skin have been preserved, sometimes in a remarkable state, by artificial post-mortem treatments (mummification) or very specific natural conditions (bodies found in bogs, ices and deserts, partially carbonized bodies). Hair has the ability to absorb and store metal ions, the origin of which can be endogenous (in nascent hair from the bulb) or exogenous. In numerous burial contexts, the presence of metal cations, which were fixed by the tissues, may have played a determinant role, as exemplified by the preservation of mineralized samples of hair, skin and textiles in close contact with metal objects. Among the most ancient keratinized fibers studied, analysis of mammoth hairs in the 1970s showed the presence of diffraction reflections indicating the preservation of α-keratin macromolecular organization (Gillespie, 1970; Ryder, 1974). They nevertheless showed a disruption of disulphide bridges and partial oxidation of keratin cysteine residues to cysteic acid.

Hairs from Egyptian mummies allow the study of specimens stored under very stable conditions, in the absence of light and humidity. Mummy hairs have been the subject of recurrent investigation since the 19th century. Over the last 40 years, progress in optical and scanning electron microscopy has enabled the detection of the oxidation of cuticle and cortex keratin (Brothwell & Spearman, 1963; Hrdy, 1978) and allowed cuticle degradation to be visualized (Chiarelli *et al.*, 1970). Hairs from the mummy of Ramses II were studied using several spectroscopic, microscopic and structural methods (Balout, 1985). More recently, hairs from two South American mummies were studied by X-ray diffraction techniques and showed a good, yet variable, preservation of keratin packing (Busson, 1998).

Use of microbeam techniques to study hair strands is reported in previous works for dermatological, cosmetological and forensic investigation using synchrotron X-ray and infrared techniques, as well as imaging by proton- and electron-induced X-ray emission (Toribara *et al.*, 1982; Malmqvist *et al.*, 1983; Forslind *et al.*, 1985; Bos *et al.*, 1985; Bantignies *et al.*, 1998; Busson *et al.*, 1999; Kamijo *et al.*, 2002; Mérigoux *et al.*, 2003).

Here we present information regarding the long-term alteration of human hair using synchrotron microfocus techniques in the X-ray and infrared spectroscopic ranges. Extensive use of microbeam techniques has been performed on these ancient samples, leading to new results about their preservation state and ageing mechanism. The origin of the trace elements quantified in these series of mummy hairs is discussed.

2. Method

We collected hair strands from two Egyptian mummies from the Greco-Roman period, preserved respectively by the museums of Archéologie Méditerranéenne of Marseille and Ignon-Fabre of Mende in France.

Hair cryomicrotomy was performed using polyvinyl alcohol/polyethylene glycol as the embedding medium (OCT, Tissue-Tek). Sample-containing blocks were solidified using liquid nitrogen, unmolded and cut with a Bright microtome. Cuts were deposited directly on sample holders for synchrotron analysis and for optical and scanning electron microscopy.

2.1. Diffraction analyses

The packings of keratin intermediate filaments and organized lipids were probed by small-angle X-ray diffraction (XRD).

XRD experiments on hair strands were performed on beamline D43 at the LURE (Orsay, France). A dozen similar hairs were aligned in a 1 mm-diameter glass capillary. The sample–detector distance was set to small angles (333 mm) and wide angles (110 mm) with a 1.45 Å wavelength beam. Patterns were recorded on an image plate, and numerized with a molecular dynamics scanner (100 µm × 100 µm resolution).

Further XRD experiments were performed on the microfocus beamline ID13 at the ESRF (Grenoble, France) using a 5 µm-diameter beam (Engström *et al.*, 1995). A high-intensity monochro-

† Current affiliation: Department of Biochemistry, University of Cambridge, 80 Tennis Court Road, CB2 1GA, Cambridge, UK.

matic beam (wavelength 0.975 Å) was focused using an ellipsoidal mirror and then reduced to 5 µm diameter by a collimator placed in the focal plane. Hair samples were stretched perpendicularly to the beam on a motorized frame mounted on a goniometer head. Samples were translated before the beam in 10 µm steps (Busson *et al.*, 1999). The sample–detector distance was set to 180 mm, accurately measured using silver behenate diffraction rings ($d_{\langle 001 \rangle}$ = 58.38 Å). Images were collected on a MAR-CCD camera (2048 × 2048 pixels, 64.45 µm × 64.45 µm resolution, 16-bit coding).

Experimental patterns were processed using *FIT2D* software for fiber diffraction analysis (Hammersley, 1989).

2.2. Local structure and conformation analyses

Infrared microscopy was performed on the MIRAGE-SA5 beamline at the LURE, using a Magna 560 bench FTIR spectrometer (Polack *et al.*, 1999). The beam was size-limited by a square aperture of 3 µm × 3 µm or 6 µm × 6 µm and each hair section was mapped using a step equal to the aperture size. The absorption signal on a 3 µm-thick hair section was collected using a MCT (mercury cadmium telluride) detector. Spectra were collected at 8 cm^{-1} resolution and averaged over 128 scans. They were displayed in the 800–4000 cm^{-1} frequency region.

OMNIC software was used for data analysis. In the infrared maps, we integrated the region from 2765 to 3015 cm^{-1} for the alkyl band (νCH_2 and νCH_3 modes) and the region from 1575 to 1805 cm^{-1} for the amide I and II bands (mainly δNH, νCN and νCO modes) (Panayiotou & Kokot, 1999). The α/β amide map was determined from the ratio of 1645–1665 cm^{-1} over 1620–1630 cm^{-1} integrated intensities in the amide I band (mainly νCO). The intensity of these bands was shown to be closely related to the quantity of amino acids involved in the corresponding conformation in protein secondary structure (Surewicz & Mantsch, 1988; Dong *et al.*, 1990).

2.3. Elemental analyses

The elemental composition of lead-treated hairs was studied using synchrotron X-ray fluorescence (XRF) at an excitation energy of 17 keV for multi-elemental analysis.

XRF longitudinal elemental analysis was performed on beamline D15 at the LURE synchrotron (Orsay, France) with a flux of 10^{10} photons s^{-1}, a 1 mm-diameter beam and an exposure time of 10 min. Each experimental measurement was repeated nine times, on three points of each of three hairs analyzed for both mummies.

This bulk analysis was detailed by XRF elemental mapping within 30 µm-thick hair sections. These measurements were carried out on beamline ID22 at the ESRF (Grenoble, France) with a focused beam of 2 µm × 5 µm (Bohic *et al.*, 2001). The flux was 5×10^{10} photons s^{-1} on the sample and the acquisition time was set to 2 s per point. Under these conditions, the lower limit of detection was of the order of 0.5 µmol g^{-1} of hair for lead and 2 µmol g^{-1} for calcium. The fluorescence data were processed using the software *WAPI* (Chevallier *et al.*, 1993) and *AXIL* (Espen *et al.*, 1987).

3. Results

We have examined the preservation of these ancient hairs from both ends of the length scale and observed a remarkable conservation of keratin packing at both the macroscopic and molecular level.

3.1. Preservation of keratin structure at all length scales

The observation under optical microscope shows the conservation of general fiber characteristics down to the micrometer scale. We observe on the surface of the hairs the presence of an organic material, the composition of which was not investigated. Electron microscopy enables us to check the state of preservation of the hair surface for both mummies. At the places where they are not covered by the organic product mentioned previously, the cuticle scales are perfectly observable although their edges appear to be notched.

The broken extremity of a hair from the Mende museum mummy, observed using scanning electron microscopy, shows the internal structure of the fiber. The diameter of the observed features (2–3 µm) suggests that these are the hair cells (see Fig. 1).

Hair diffraction images from both mummies show the preservation of the molecular and supramolecular structure of fibrillar keratins. The keratin α-helical structure (sharp axial arc at 5.15 Å), the coiled coil (broad equatorial spots centered at 9.8 Å and axial repeat of the 470 Å fundamental reflection), as well as the intermediate filament assembly (equatorial harmonics at 88 Å), are at least as remarkably evidenced as in a native sample diffraction pattern (see Fig. 2).

The fine structure of the axial arc at 5.15 Å, with off-axis reflections around 5 Å, is also present, which confirms the high-resolution

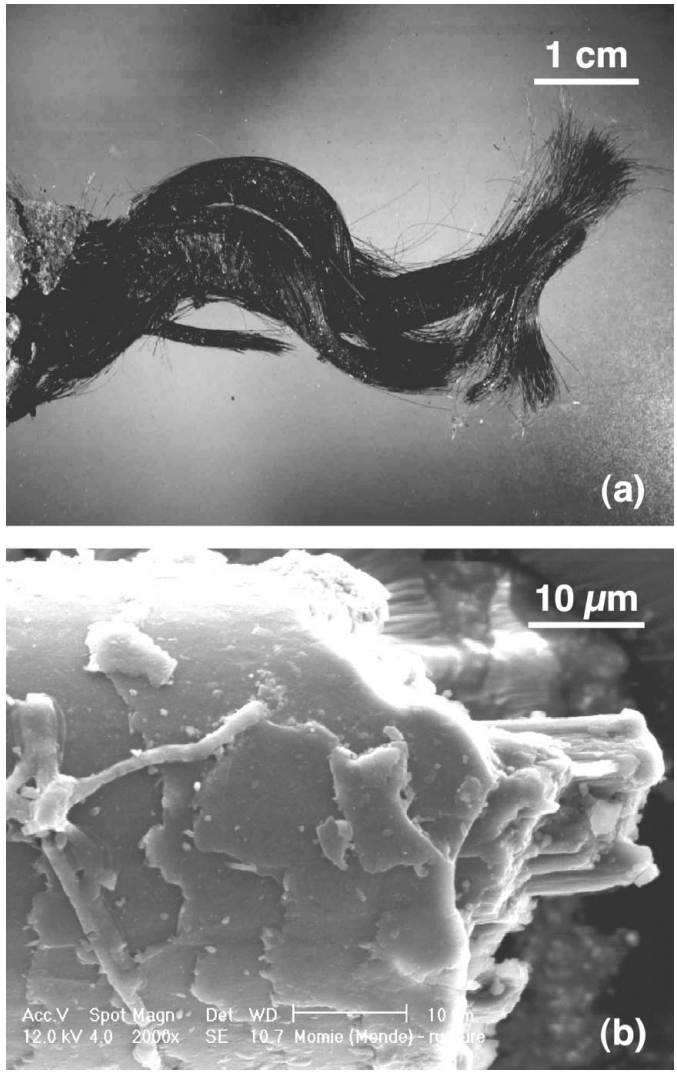

Figure 1
(*a*) Lock of mummy hair from the Greco-Roman period (Mende museum), total length approximates 7 cm. (*b*) Scanning electron microscopy image of a section of hair from the Mende museum mummy. Ancient hair cells appear at the place of the cut.

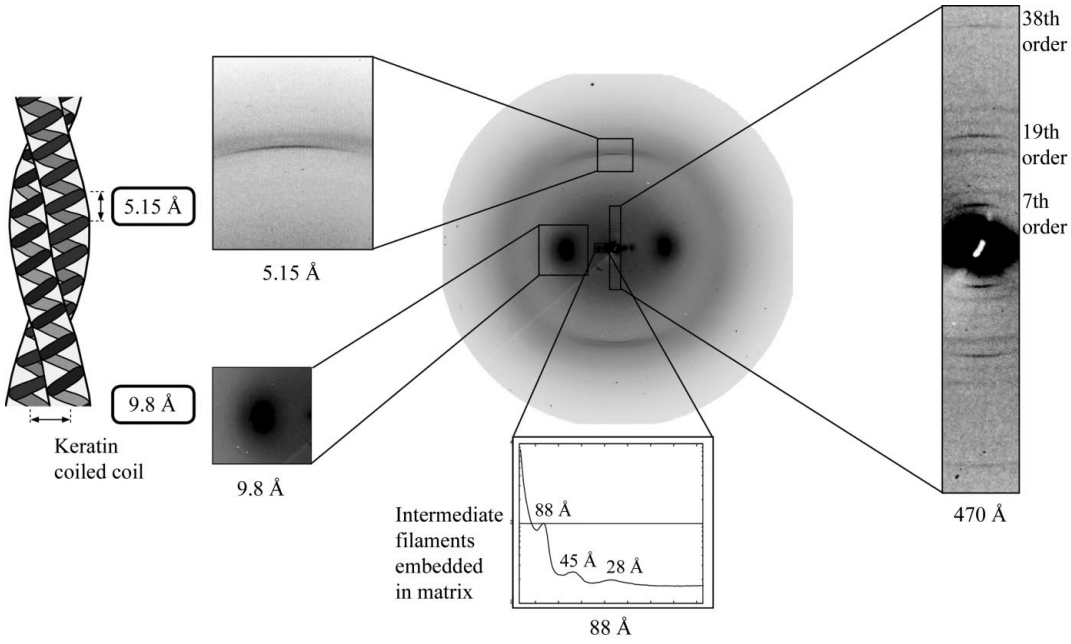

Figure 2
Small-angle X-ray diffraction image of a hair from the Marseille mummy. Insets show the reflections corresponding to the major α-keratin structure features. See Fig. 3 for details on intermediate filament organization.

preservation of the α-helices (at less than 0.1 Å). These experiments attest to the conservation of hair keratin structure at any observed supramolecular length scale. Unexpectedly, the comparison with native hair shows an even stronger contrast of certain diffraction features. Harmonics corresponding to the fundamental reflections at 88 Å and 470 Å appear strongly reinforced.

The lipid diffraction rings generally present in the diffraction pattern of native samples are not observed for these ancient hairs. This suggests that the organized lipid fraction has been destroyed or disorganized during the 2000 year ageing process.

3.2. Long-term modifications of proteacinous matrix and embedded intermediate filaments

We studied more particularly the harmonics of the spot centered at 88 Å, which corresponds to the average distance between intermediate filaments in the hexagonal paracrystalline lattice. The analysis of these reflections is facilitated compared with native hair samples owing to the absence of lipid diffraction rings.

We fitted the data using small-angle diffraction models. In a new model we built a centrosymmetric bidimensional paracrystalline lattice at $2\pi/3$ and averaged it with a threefold symmetry (Hosemann & Bagchi, 1962; Bertrand, 2002). Other models have recently been proposed, based on the direct construction of a hexagonal paracrystalline lattice (Briki *et al.*, 1998).

Both models are consistent with our experimental data. From 300 to 12 Å, the intensity of the continuous background is precisely fitted by a power function of the wavenumber (exponent *ca* -2.78). The exponent value exceeds the value observed by Briki *et al.* (1998) in native hair by more than 20%. It is to be noted that various parameters can modulate the central diffusion, including the contribution of amorphous keratins (Busson, 1998), microporosity (Balout, 1985) and the average electronic density of the material (strongly influenced by heavy metal content).

Peak positions are correctly reproduced by the models (see Fig. 3). Differences in the intensities are probably due to an excessive simplification in the choice of the form factor of the intermediate filaments (hard core model), as pointed out for native hair strands (Briki *et al.*, 1998). The hard core radius of the intermediate filament (r_{ext}), the Gaussian standard deviation characterizing the paracrystalline network (σ) and the distance between intermediate filaments (D) remain identical between native and Marseille mummy hairs. According to these simplified diffraction models of the intermediate filaments organization, the relative volume (49%) of the intermicrofibrillary matrix does not vary significantly between ancient and native samples.

The intermediate filaments organization in the proteacinous matrix would therefore not have been sensibly modified after a two-millennia ageing. Therefore, our diffraction data indicate that neither a long-term contraction of the amorphous matrix nor a significant reorganization of the intermediate filaments occurred in the long-term desiccating atmosphere.

3.3. Local structure and conformation from infrared microscopy

We carried out the synchrotron infrared microscopy of hair sections from both mummies (see Fig. 4) and focused mainly on bands resulting from alkyl and amide groups.

The νCH map enables us to precisely localize hair section contour. Signals of bands νCH_2 and νCH_3, mainly originating from hair keratin alkyl groups, are almost constant on the whole map. The absence of the usually observed lipid peak at the centre of the map (Bantignies *et al.*, 1998; Kreplak *et al.*, 2001) is noteworthy. Indeed, variance among map spectra shows that only the amide I and amide II bands vary in a significant way across the map.

The amide band map shows a very strong decrease of the amide I signal from the centre of the hair to its periphery (by a factor of four approximately). This observation differs from former results and our data on native hair, where amide band intensity was shown to remain almost constant all over the cortex area (Bantignies *et al.*, 1998; Bertrand, 2002). This strongly indicates a long-term modification of the proteic fraction at the hair periphery through partial disruption of the polypeptide backbone.

Moreover, the (α/β) ratio decrease in the amide I band towards the hair periphery indicates subsequent conformational changes for remaining polypeptide chains into disordered α-helices.

3.4. Metal ion distribution

Elemental analysis of these mummy hairs, compared with native modern hairs, shows a significant trace increase in element content.

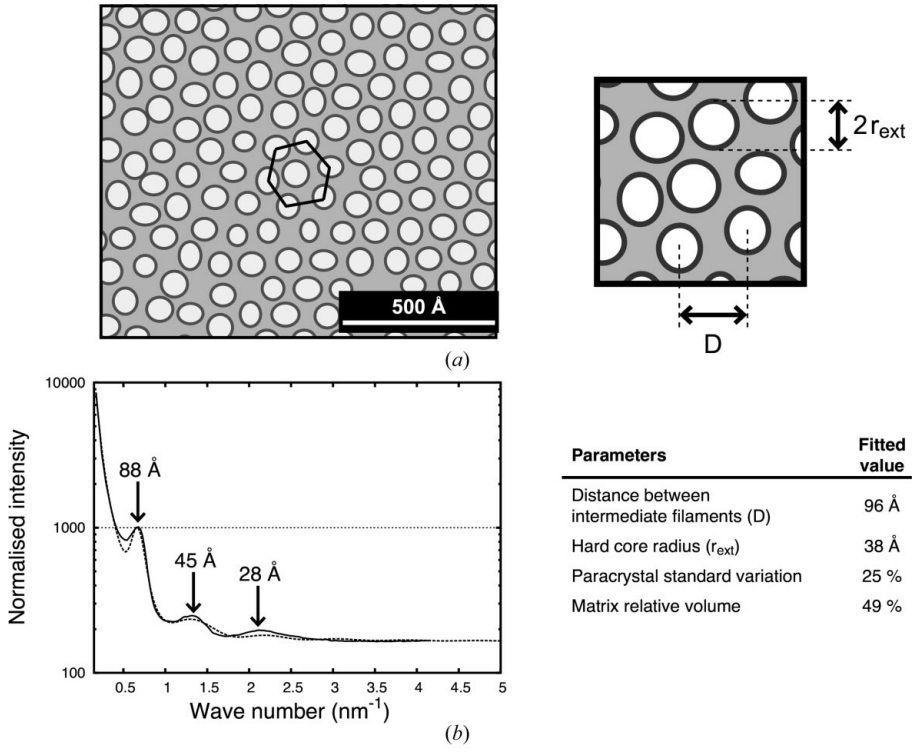

Parameters	Fitted value
Distance between intermediate filaments (D)	96 Å
Hard core radius (r_{ext})	38 Å
Paracrystal standard variation	25 %
Matrix relative volume	49 %

Figure 3
(*a*) Contours extracted from a transmission electron microscopy image of wool cortex from Rogers (1959), showing the hexagonal distorted packing of the intermediate filaments. (*b*) Integrated intensity (plain line) from 300 Å to 12 Å and fit of maxima positions using a symmetrized paracrystalline model.

Elemental distribution across the hair section differs noticeably between Mende and Marseille hair strands.

3.4.1. Mende museum elemental analysis. X-ray fluorescence study of Mende mummy hair strands shows a notable increase in calcium (146 μmol g^{-1} on average), zinc (37 μmol g^{-1}), iron (14 μmol g^{-1}) and lead (1.1 μmol g^{-1}) contents, compared with maximum contents observed in native samples (Valković, 1998). Some other elements of lower occurrence in native hair such as manganese (1.8 μmol g^{-1}), bromine (1.1 μmol g^{-1}), titanium (1.1 μmol g^{-1}) and strontium (0.62 μmol g^{-1}) show a significant increase.

Preliminary X-ray absorption experiments at the zinc edge on LURE beamline D21 show that EXAFS spectra collected on Mende hairs differ noticeably from those obtained on native hair. The environment of Zn atoms would thus be different. We can therefore suppose that the endogenous zinc environment was modified during long-term preservation or, more probably, that the abundant exogenous Zn atoms would have been fixed in a different environment from that of metabolic Zn atoms.

3.4.2. Marseille mummy elemental analysis. Element distribution across a hair section from the Marseille mummy, determined by synchrotron microfluorescence analysis, shows a very heterogeneous distribution (see Fig. 5). The localization of S atoms, mainly originating from hair proteins, enables a clear determination of the hair section contour.

We distinguish three distinct schemes for elemental distribution:

(i) Some elements are distributed in the fiber section as in current hair: calcium in the medulla (Mérigoux *et al.*, 2003);

(ii) Others are concentrated specifically in some of the histological zones: in the medullary canal (zinc, manganese, lead, strontium) and/or in a crown at the hair periphery (iron, copper and lead);

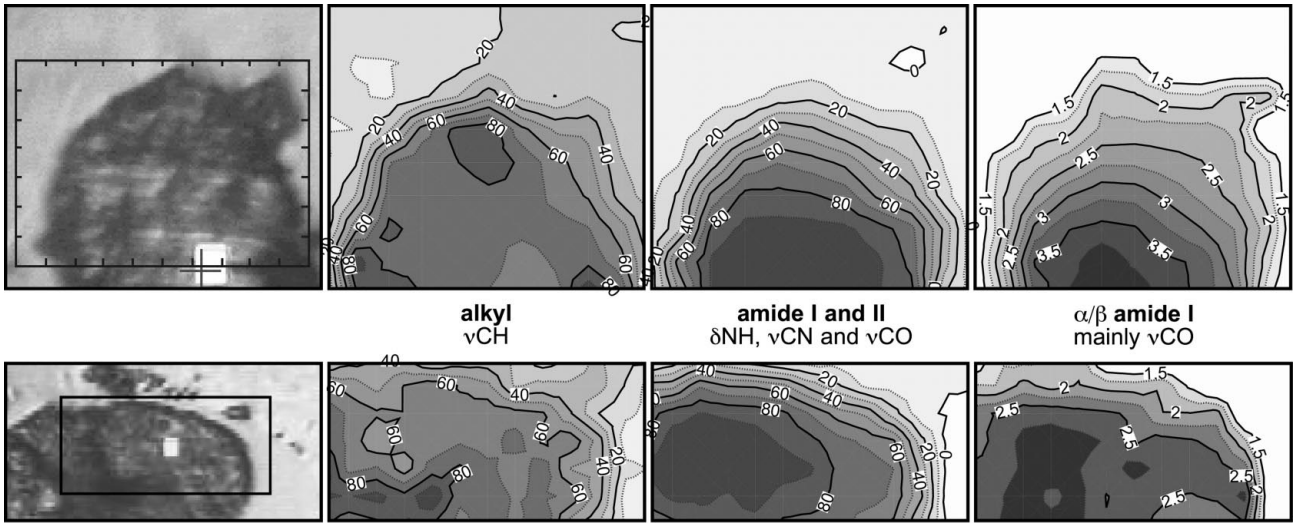

Figure 4
Microscopy images and infrared maps of hair sections from the Mende and Marseille mummies. The plain white square on the microscopy images corresponds to the beam size. Note the absorbance variation of the amide bands for both hairs, and of the amide I α/β ratio for Marseille hair. For the alkyl and amide maps, the signal is normalized to the maximum value and each step of the contour plots corresponds to a variation of 10% of this maximum. For the amide I ratio map, the signal is set to zero outside the hair contour.

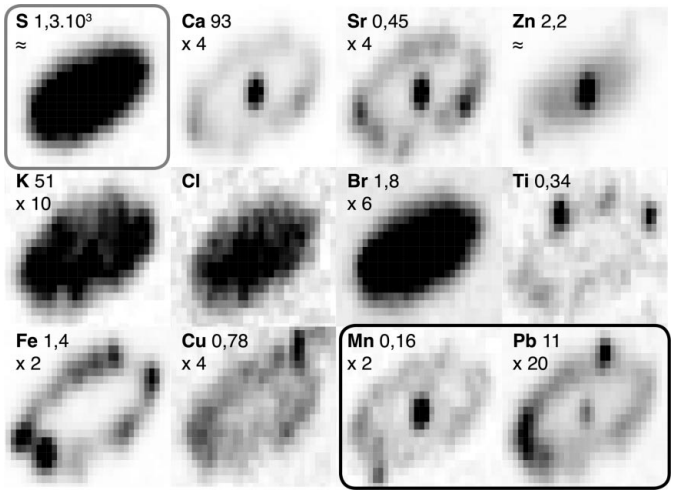

Figure 5
X-ray microfluorescence cartography of a hair section from the Marseille mummy. The elemental content is indicated in μmol g^{-1}, followed by the ratio to the average trace-element content in native hair.

(iii) We observe unambiguously the presence of impurities deposited on the hair surface (particularly titanium and zinc).

3.4.3. Discussion. Interestingly, part of the trace elements most probably originates from the mummification treatments. The *natron* used during this process was shown to be a complex mixture associating varying proportions of sodium chloride, sulfate, carbonate and bicarbonate, as well as small quantities of calcium carbonate. Significant contents of calcium and chlorine are actually observed in our samples.† All the trace elements (calcium, and its analogue strontium, bromine, chlorine, iron and magnesium) mentioned in natron samples of the Greco-Roman period (Macke *et al.*, 1997) are present in excess in Marseille mummy hair strands.

The diffusion of some of these ions in the whole section of a Marseille strand suggests that the hair could have been washed or treated with a liquid or pasty solution, unlike the body for which the solid application of natron is accepted by most of the authors. We additionally noted very high contents of manganese and lead in hair strands from both mummies, not mentioned as components of natron by Macke *et al.* (1997). These elements are particularly concentrated at the hair periphery and in the medulla of the Marseille sample. Lead and manganese content could result from cosmetic treatments. Let us recall that the use of lead-based make-up is well documented in Ancient Egypt and that the production of manganese-based hair dyes is also known (Walter *et al.*, 1999; Laskowska-Kusztal, 1978). The specific concentration of lead, calcium and other cations within the medullary canal, where the lipids were concentrated before mummification, could be related to the saponification of hair lipids (Bertrand *et al.*, 2003).

The absorption of exogenous metal cations within the fiber may have locally increased the electronic density of the material. The diffusion of metal ions can moreover have had a structuring effect by regularly organizing keratin molecules around the metal sites. This could explain the increase in contrast observed in the diffraction patterns of these ancient hairs. Note that it is improbable that the diffraction contrast increase results from the evolution towards a more organized keratin structure as, on the contrary, infrared spectroscopy experiments show a degradation of keratin chains at the molecular level.

† Sodium and magnesium are too light elements to be quantified with the X-ray fluorescence set-up used in this work.

4. Conclusion

The development of microfocus synchrotron beamlines leads to new results regarding archaeological samples of biological origin. Here, we made extensive use of microbeam techniques to study ancient hair samples, leading to new results about their preservation state and ageing mechanism. We analyzed hair samples of Egyptian mummies using a conjunction of structural and elemental synchrotron methods and discuss the long-term modification of keratinized fibers.

In these favored contexts of conservation, structural analyses reveal a remarkable preservation of keratin supramolecular organization at any observed length scale. Detailed diffraction analysis of hair intermediate filaments organization showed no sensible modification after a two-millennia ageing. Nevertheless, infrared spectroscopy indicates a partial disorganization of keratins through polypeptide bond breakage. Elemental mapping shows a very heterogeneous distribution which we can relate to mummification treatments using natron salts, as well as to ancient cosmetic habits.

We wish to thank Marine Cotte for her expertise and contribution to hair cryomicrotomy, Dr Christophe Moulherat for helpful archaeological discussions about this work and Vijay Sankaran for his re-reading of the manuscript. We are grateful to Professor Simone Benazeth, Dr Ioannis Nicolis and Dr Emmanuel Curis, Faculté de Pharmacie René Descartes, Paris, France, for their contribution to the X-ray absorption experiments at the LURE synchrotron. This work is supported by an ACI grant funded by the French Ministère de la Recherche.

References

Balout, L. (1985). *La Momie de Ramsès II, Contribution Scientifique à l'Égyptologie.* Paris: CNRS Recherche sur les Civilizations.
Bantignies, J.-L., Fuchs, G., Carr, G. L., Williams, G. P., Lutz, D. & Marull, S. (1998). *Int. J. Cosmet. Sci.* **20**, 381–394.
Bertrand, L. (2002). PhD thesis, Université Paris 6, France.
Bertrand, L., Doucet, J., Simionovici, A., Tsoucaris, G. & Walter, P. (2003). *Biochim. Biophys. Acta*, **1620**, 218–224.
Bohic, S., Simionovici, A., Ortega, R. & Snigirev, A. (2001). *Appl. Phys. Lett.* **78**, 3544–3546.
Bos, A. J. J., van de Stap, C. C. A. H., Valković, V., Vis, R. D. & Verheul, H. (1985). *Sci. Total Environ.* **42**, 157–169.
Briki, F., Busson, B. & Doucet, J. (1998). *Biochim. Biophys. Acta*, **1429**, 57–68.
Brothwell, D. R. & Spearman, R. (1963). *Science in Archaeology*, p. 427. London: Thames and Hudson.
Busson, B. (1998). PhD thesis, Université Paris 11, France.
Busson, B., Engström, P. & Doucet, J. (1999). *J. Synchrotron Rad.* **6**, 1021–1030.
Chevallier, P., Wang, J. X., Piccot, D., Legrand, F. & Abbas, K. (1993). *Proc. de la Conférence Spectrométrie γ et X*, Saint Rémy-Lès-Chevreuse, Notes CEA N-2756.
Chiarelli, B. A., Conti Fuhrman, A. & Rabino Massa, E. (1970). *Riv. Antropol.* **62**, 275–278.
Dong, A., Huang, P. & Caughey W. S. (1990). *Biochemistry*, **29**, 3303–3308.
Engström, P., Fiedler, S. & Riekel, C. (1995). *Rev. Sci. Instrum.* **66**, 1348–1350.
Espen, P. van, Janssens, K. & Nobels, J. (1987). *Chemometrics Intell. Labor. Syst.* **1**, 109–114.
Forslind, B., Grundin, T. G., Lindberg, M., Roomans, G. M. & Werner, Y. (1985). *Scan. Electron. Microsc.* **2**, 687–695.
Fraser, R. D. B., MacRae, T. P., Parry, D. A. D. & Suzuki, E. (1986). *Proc. Natl. Acad. Sci. USA*, **83**, 1179–1183.

Fraser, R. D. B., MacRae, T. P., Rogers, G. E. & Filshie, B. K. (1963). *J. Mol. Biol.* **7**, 90–91.
Garson, J.-C., Doucet, J., Lévêque, J.-L. & Tsoucaris, G. (1991). *J. Invest. Dermatol.* **96**, 43–49.
Gillespie, J. M. (1970). *Science*, **170**, 1100–1102.
Hammersley, A. P. (1989). *Synchrotron Rad. News*, **2**, 24–26.
Hosemann, R. & Bagchi, S. N. (1962). *Direct Analysis of Diffraction by Matter.* Amsterdam: North Holland.
Hrdy, D. B. (1978). *Am. J. Phys. Anthrop.* **49**, 277–282.
Kamijo, N., Suzuki, Y., Awaji, M., Takeuchi, A., Takano, H., Ninomiya, T., Tamura, S. & Yasumoto, M. (2002). *J. Synchrotron Rad.* **9**, 182–186.
Kreplak, L., Briki, F., Duvault, Y., Mérigoux, C., Leroy, F., Lévêque, J.-L., Miller, L., Carr, G. L., Williams, G. P. & Dumas, P. (2001). *Int. J. Cosmet. Sci.* **23**, 369–374.
Laskowska-Kusztal, E. (1978). *Études et Travaux*, Vol. 10, pp. 83–120. Centre d'Archéologie Méditerranéenne de l'Acad. Polonaize des Sciences.
Macke, A., Macke-Ribet, C. & Morcellet, M. (1997). *Memnonia*, **8**, 197–210.
Malmqvist, K. G., Carlsson, L. E., Akselsson, K. R. & Forslind, B. (1983). *Scan. Electron Microsc.* **4**, 1815–1825.
Mérigoux, C., Briki, F., Sarrot-Reynauld, F., Salomé, M., Fayard, B., Susini, J. & Doucet, J. (2003). *Biochim. Biophys. Acta*, **1619**, 53–58.
Panayiotou, H. & Kokot, S. (1999). *Anal. Chim. Acta*, **392**, 223–225.
Polack, F., Mercier, R., Nahon, L., Armellin, C., Marx, J. P., Tanguy, M., Couprie, M. E. & Dumas P. (1999). *Proc. SPIE*, **3775**, 13–21.
Rogers, G. E. (1959). *J. Ultrastruct. Res.* **2**, 309–330.
Ryder, M. L. (1974). *Nature (London)*, **249**, 190–192.
Surewicz, W. K. & Mantsch, H. H. (1988). *Biochim. Biophys. Acta*, **952**, 115–130.
Toribara, T. Y., Jackson, D. A., French, W. R., Thompson, A. C. & Jaklevic, J. M. (1982). *Anal. Chem.* **54**, 1844–1849.
Valković, V. (1988). *Human Hair*, Vol. 2. Boca Raton: CRC Press.
Walter, P., Martinetto, P., Tsoucaris, G., Bréniaux, R., Lefebvre, M. A., Richard, G., Talabot, J. & Dooryhée, E. (1999). *Nature (London)*, **397**, 483–448.

 Received 24 March 2003 • Accepted 7 July 2003